Supplementary material to:

"Evaluating the physical and biogeochemical state of the global ocean component of UKESM1 in CMIP6 Historical simulations", submitted to *Geosci. Mod. Dev.*

Andrew Yool et al.

National Oceanography Centre, European Way, Southampton SO14 3ZH, UK

October 30, 2020

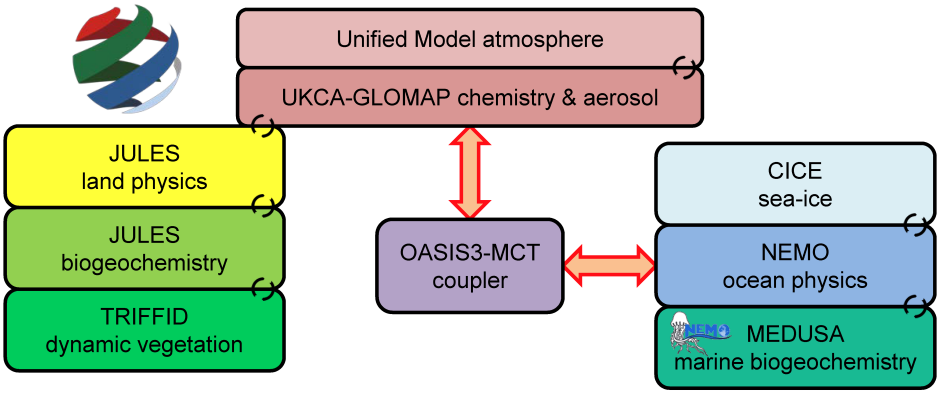

Figure S1. Schematic diagram of the components of UKESM1 and the associated code structuring and coupling relationships. Circular arrows indicate couplings between closely associated component codes, while large arrows indicate couplings between separate and distinct component codes (principally the atmosphere and ocean).

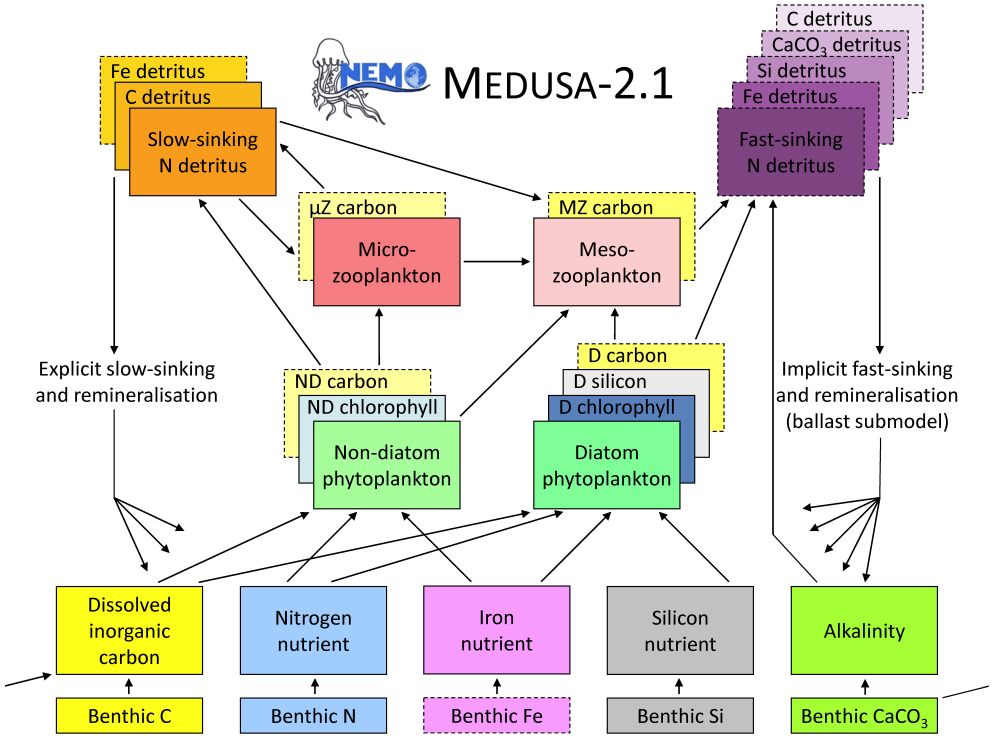

Figure S2. Schematic diagram of the MEDUSA-2.1 marine biogeochemistry model, showing both its components and their linkages. The model includes the biogeochemical cycles of nitrogen, silicon, iron, carbon, alkalinity and oxygen in a dual size class nutrient-phytoplankton-zooplankton-detritus framework. Components with solid borders are those explicitly represented as passive tracers in MEDUSA-2.1, while those with dashed borders are implicit to reduce model cost. These are either linked via rigid stoichiometry to explicit components (e.g. carbon in plankton) or occur only temporarily (e.g. fast-sinking detritus). Oxygen has been omitted from the diagram for simplicity.

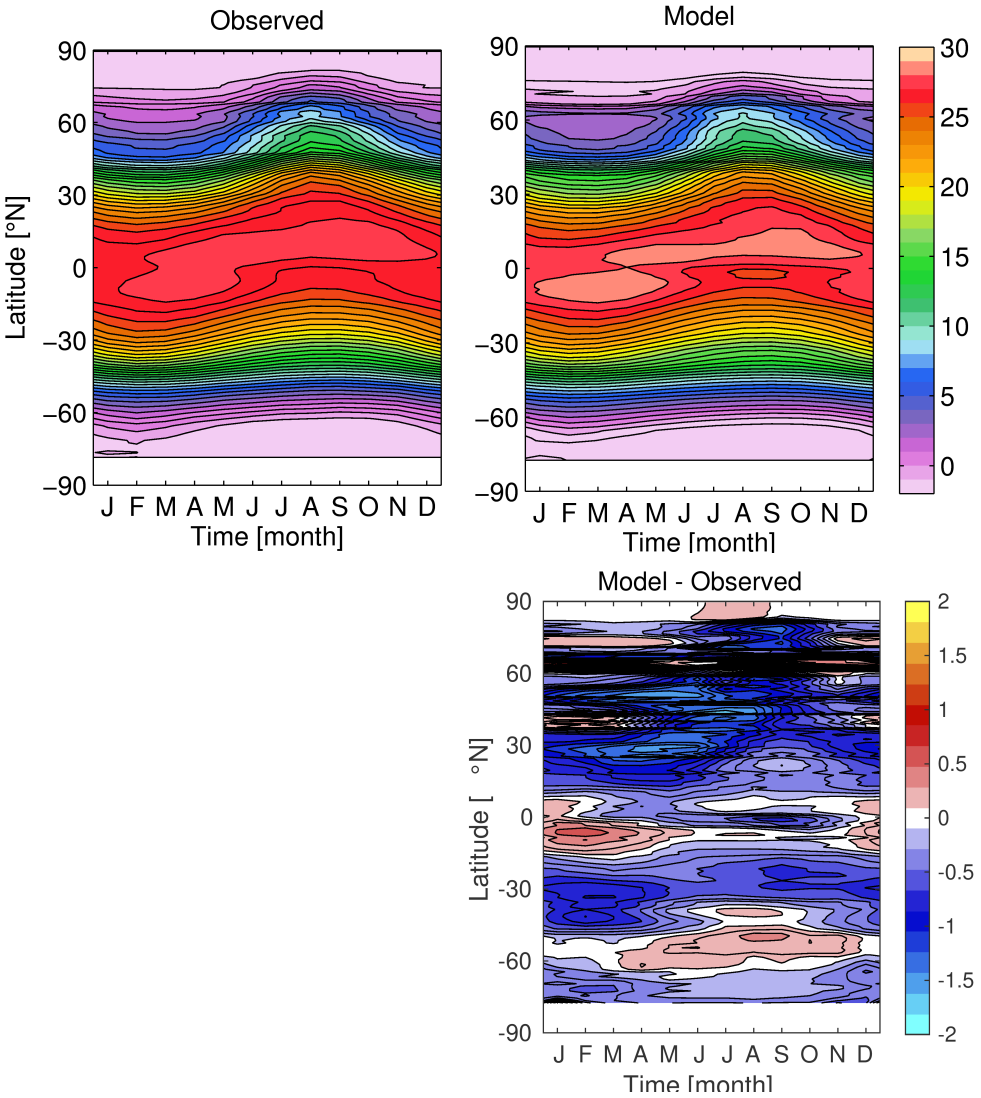

Figure S3. Observed (left; HadISST) and simulated (right) Hovmöller diagrams of sea surface temperature (in °C).

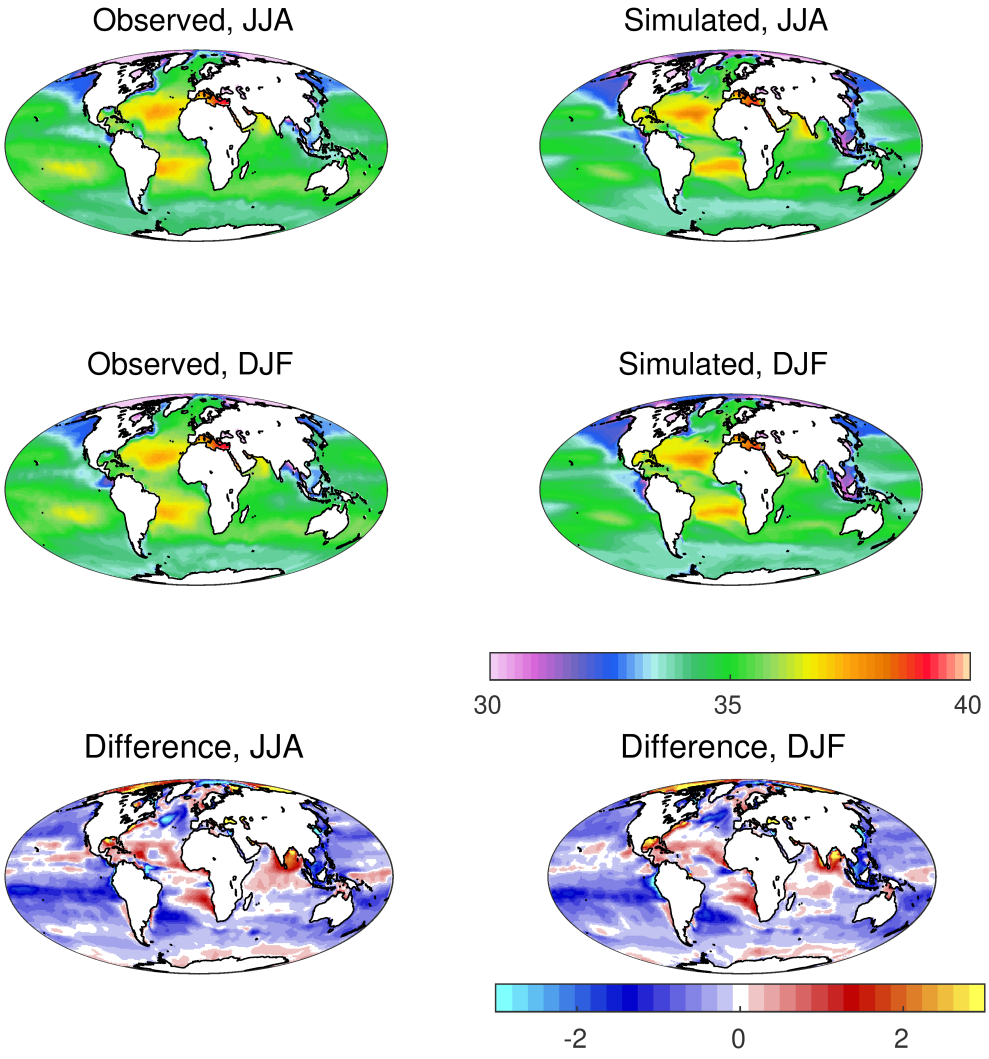

Figure S4. Observational (WOA, 2013) and simulated sea surface salinity for northern (top; JJA) and southern (medium; DJF) summer. Differences (simulated - observed) for both seasons shown in bottom row. Salinity (and difference in salinity) in PSU.

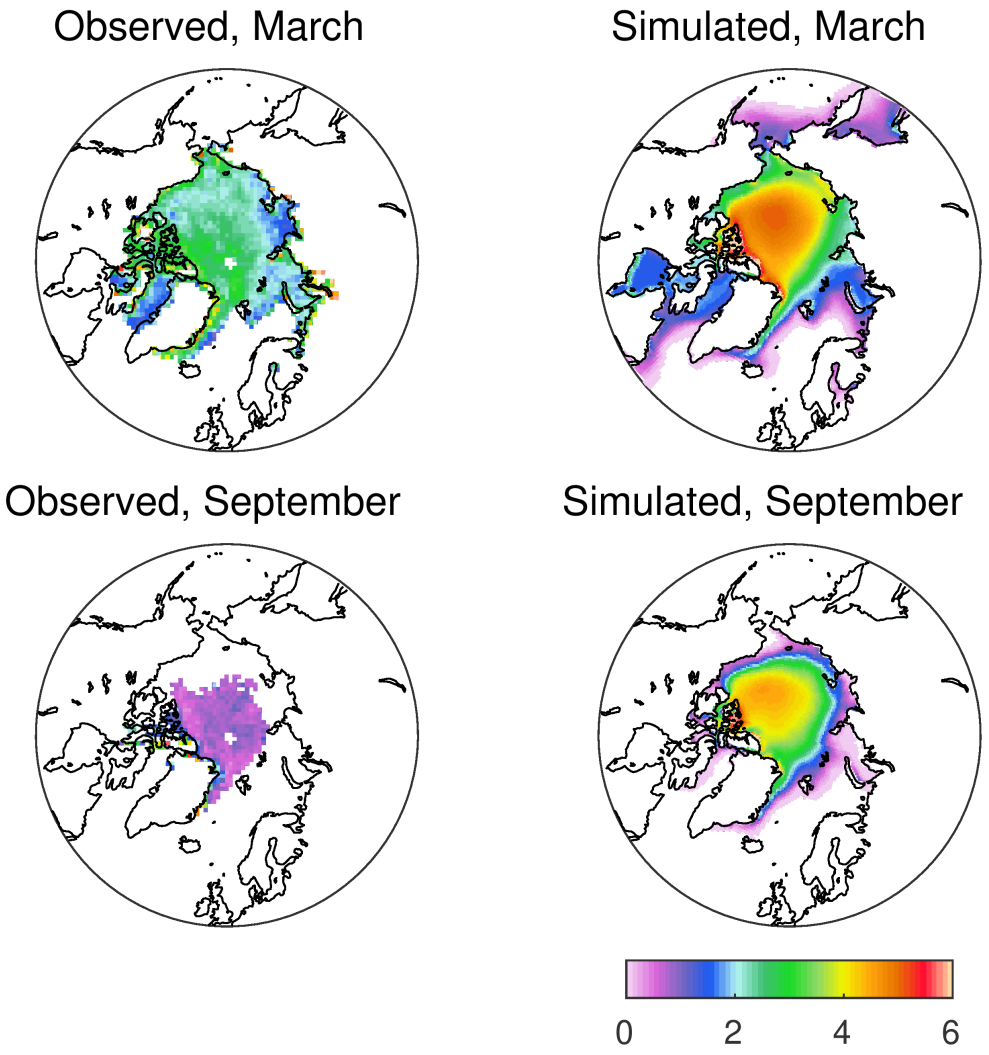

Figure S5. Observational (left; NSIDC) and simulated (right) maximum (top; March) and minimum (bottom; September) sea-ice thickness for the Arctic. Model sea-ice thicknesses of less than 0.01 m have been masked. Sea-ice thickness is in m.

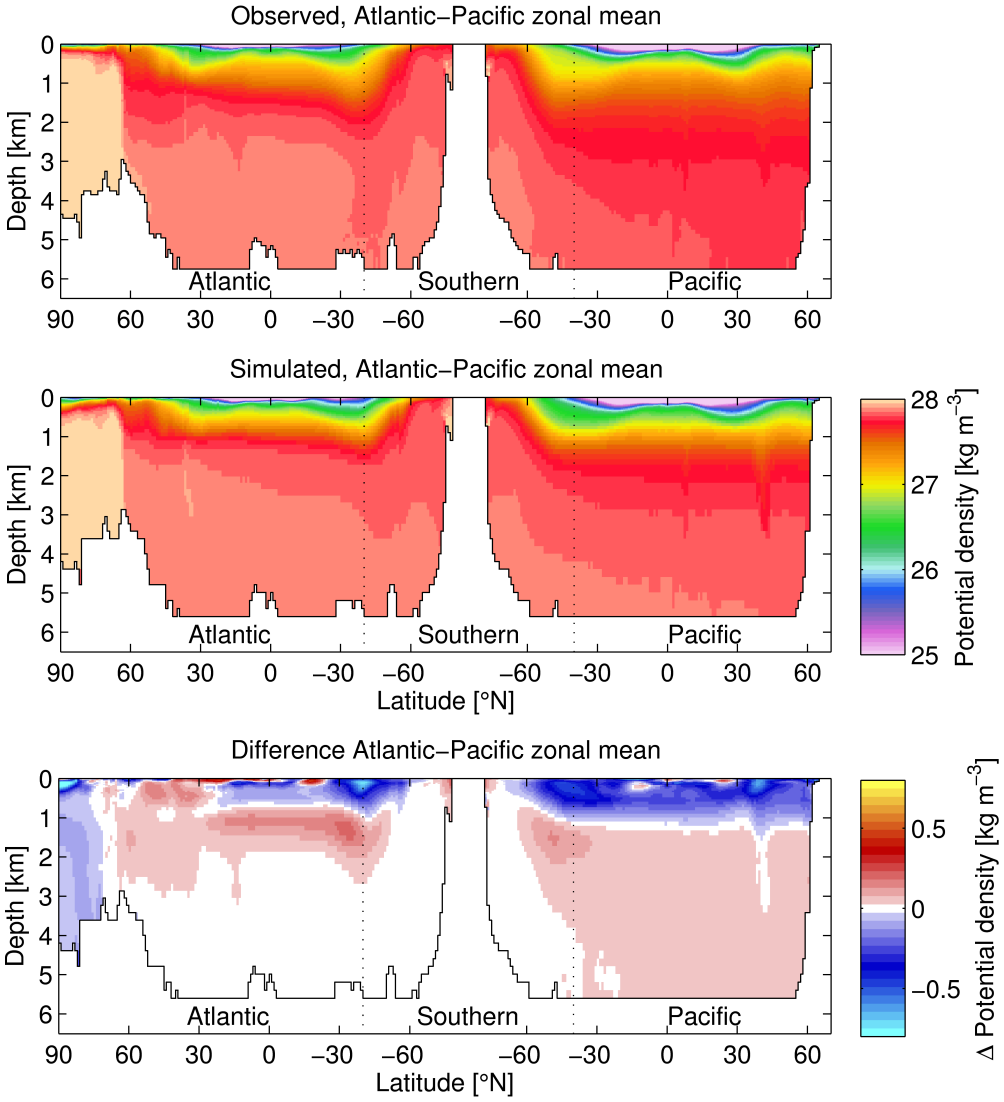

Figure S6. A "thermohaline circulation" section of observed (top) and modelled (bottom) zonal potential density anomaly (σ_θ; referenced to atmospheric pressure). Figure 6 explains the format of this section. Potential density anomaly in kg m^{-3} (minus 1000 kg m^{-3}).

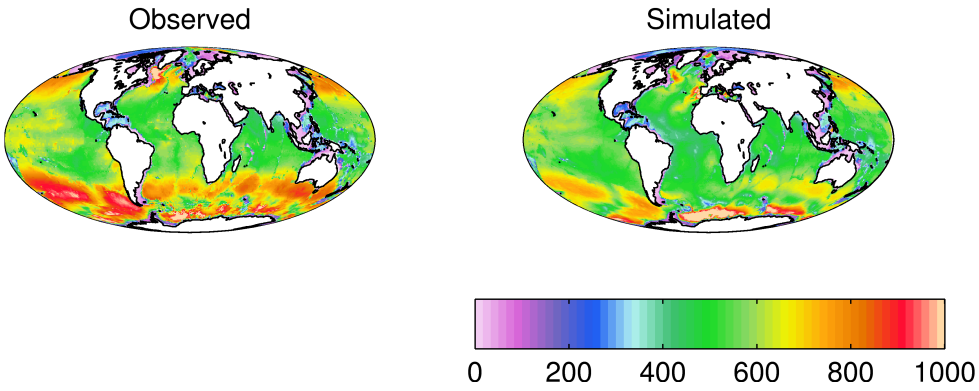

Figure S7. Observationally-derived (left; World Ocean Atlas) and simulated (right) annual average pycnocline depth. Depth derived using the Gnanadesikan et al. (2002) methodology and full three-dimensional fields of potential temperature and salinity. Pycnocline depth in m, and shown on a linear scale.

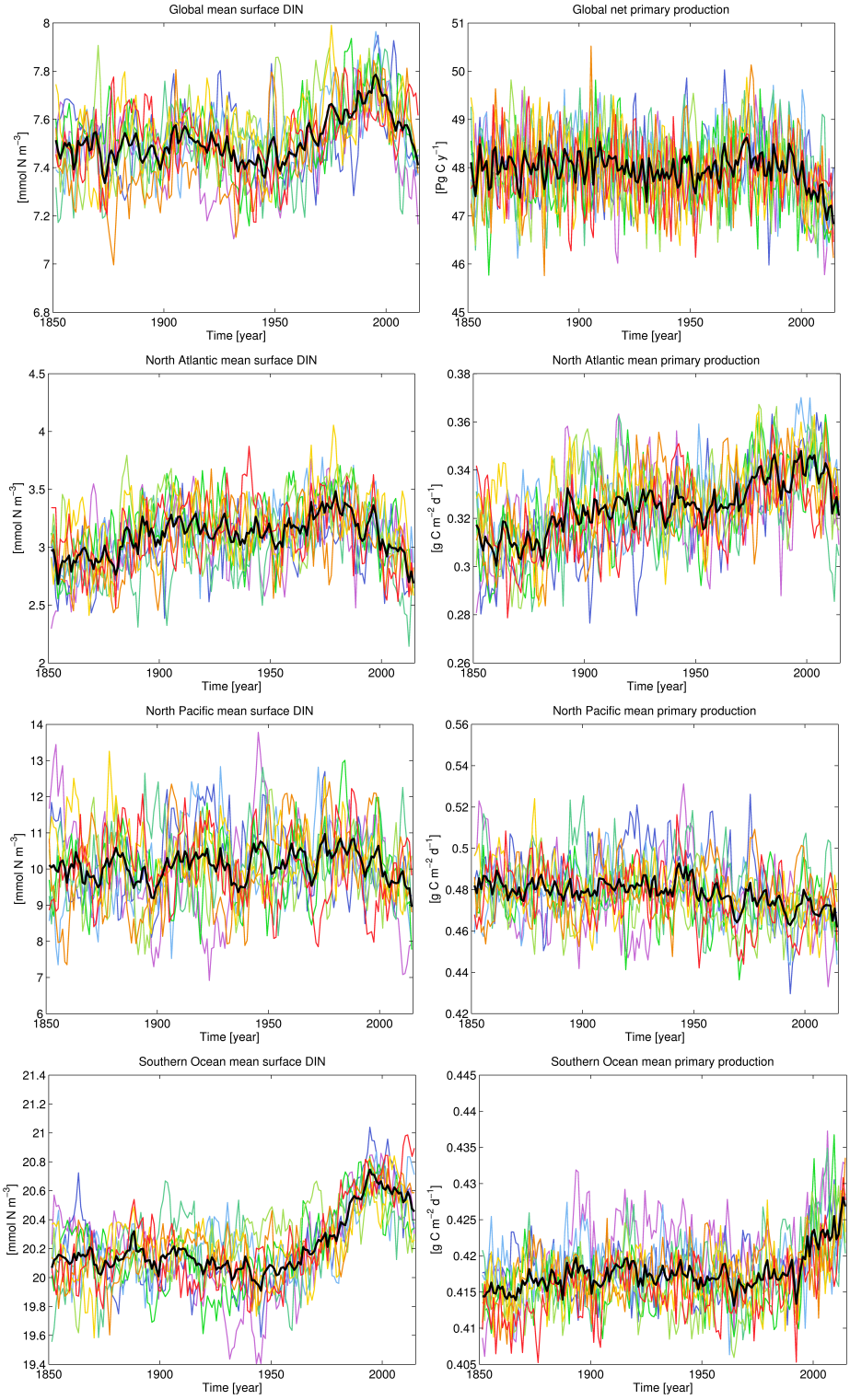

Figure S8. Time-series plots of mean surface DIN (left) and vertically–integrated primary production (right) during the Historical period from 1850 to 2015. Time-series are shown for global (row 1), North Atlantic (row 2), North Pacific (row 3) and Southern Ocean (row 4) regions. Panels show annual averages for all 9 ensemble members (coloured lines) and the ensemble mean (solid black line).

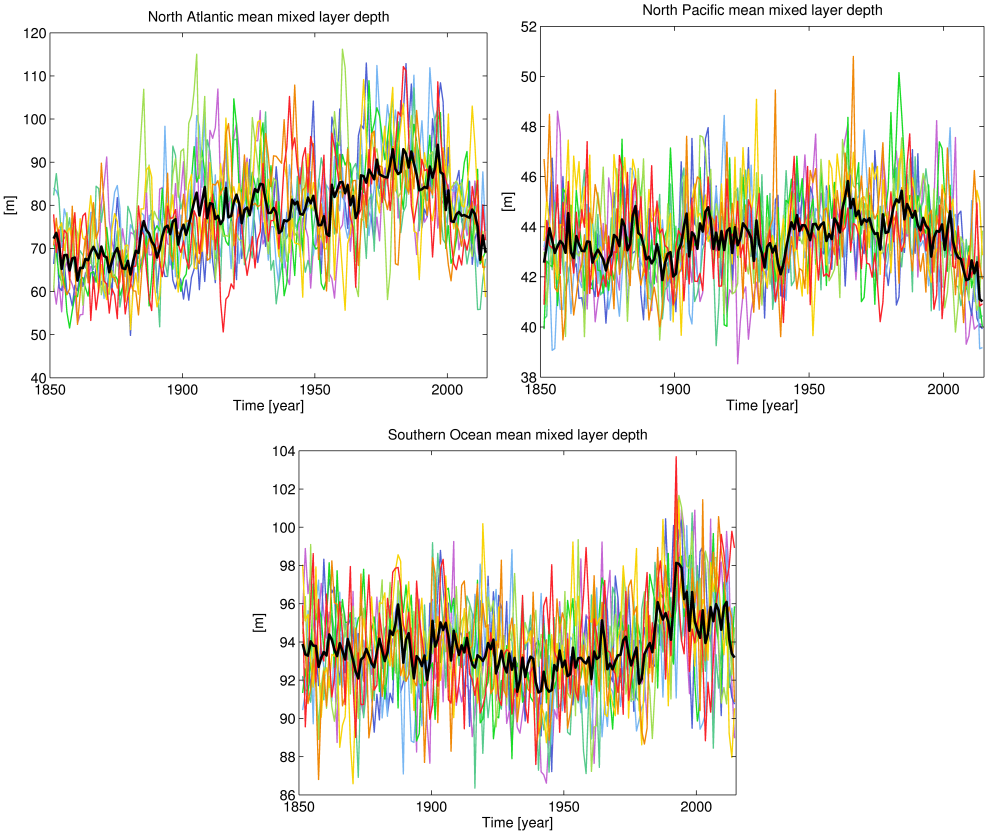

Figure S9. Time-series plots of mean mixed layer depth for the main productive biomes during the Historical period from 1850 to 2015. Panels show annual averages for the North Atlantic (top left), North Pacific (top right), and Southern Ocean (bottom). All 9 ensemble members are shown (coloured lines), together with the ensemble mean (solid black line).

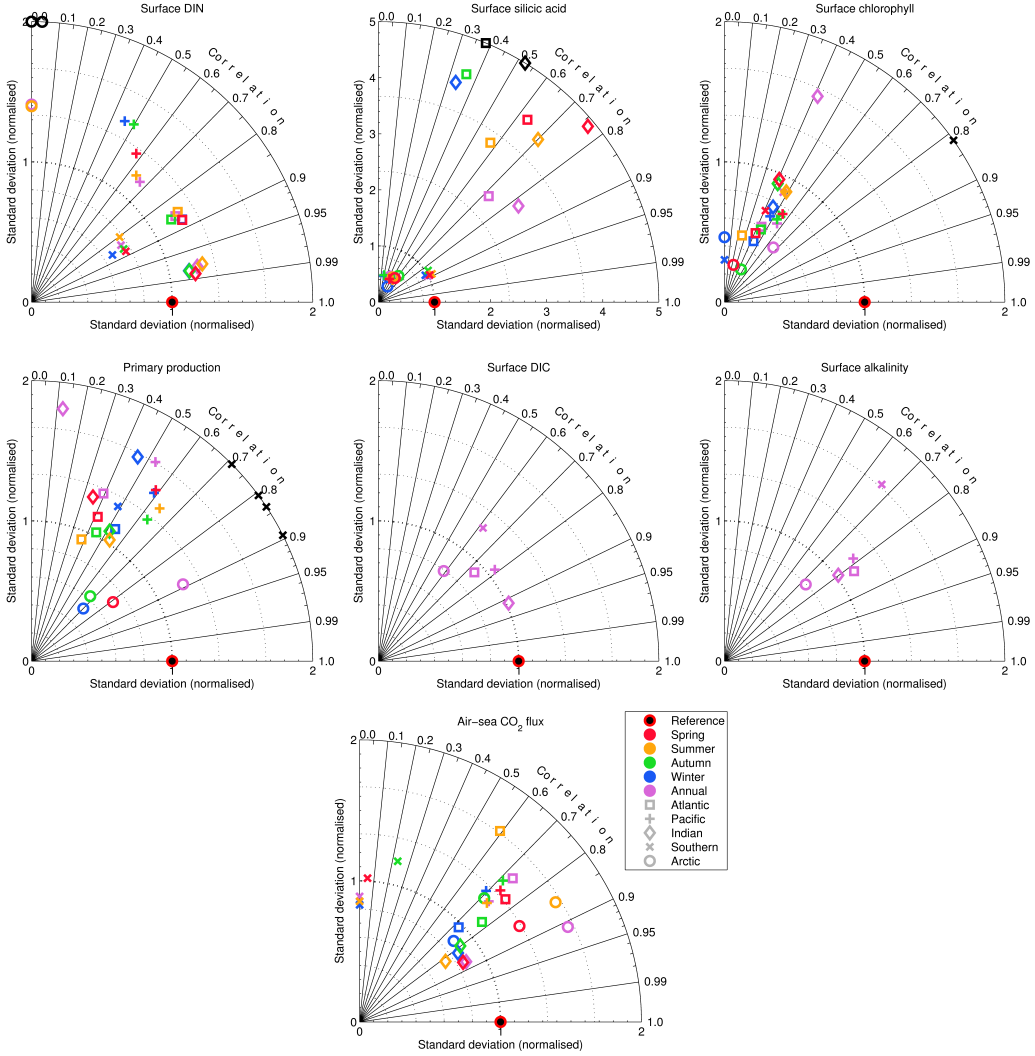

Figure S10. Taylor diagrams illustrating the seasonal and regional skill of UKESM1 over the set of standard surface ocean of biogeochemical properties: DIN (row 1, left), silicic acid (row 1, centre), chlorophyll (row 1, right), primary production (row 2, left), DIC (row 2, centre), alkalinity (row 2, right) and air-sea CO_2 flux (row 3). The diagrams share a common model key (row 3).

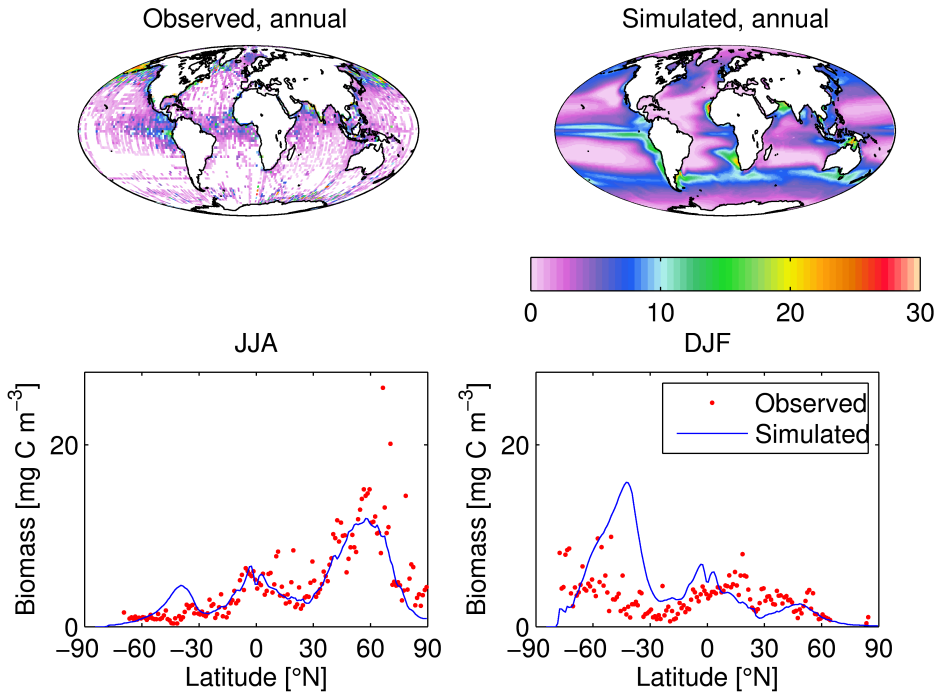

Figure S11. Annual mean observed (top left) and simulated (top right) mesozooplankton biomass, together with latitudinal averages for northern summer (bottom left; JJA) and southern summer (bottom right; DJF). Concentrations in mg C m^{-3}.

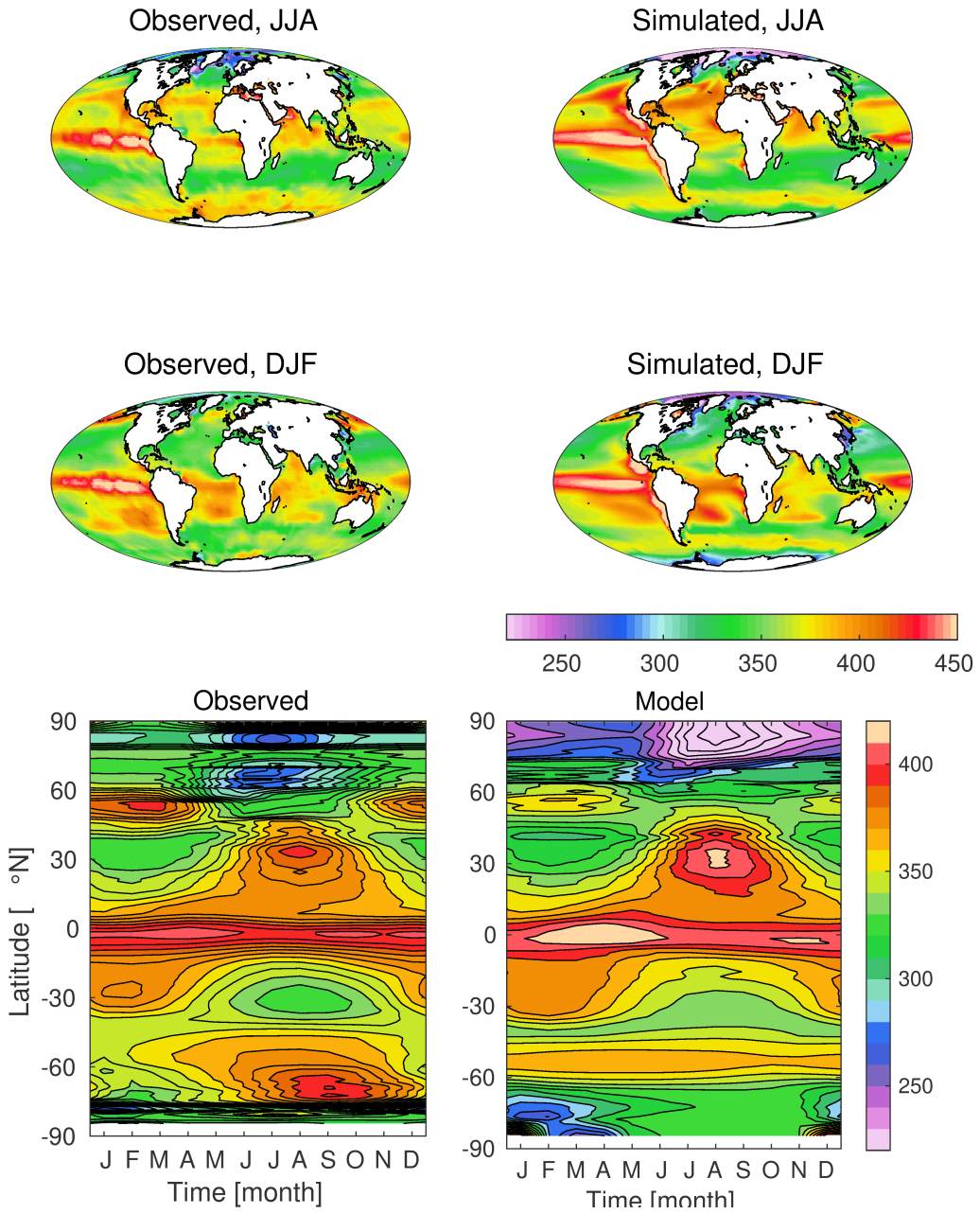

Figure S12. Observed (left; Rödenbeck et al. (2013)) and simulated (right) surface carbon dioxide partial pressure, shown geographically for northern (top; JJA)and southern summer (middle; DJF), and as zonal Hovmöller diagrams (bottom). pCO_2 in μatm.

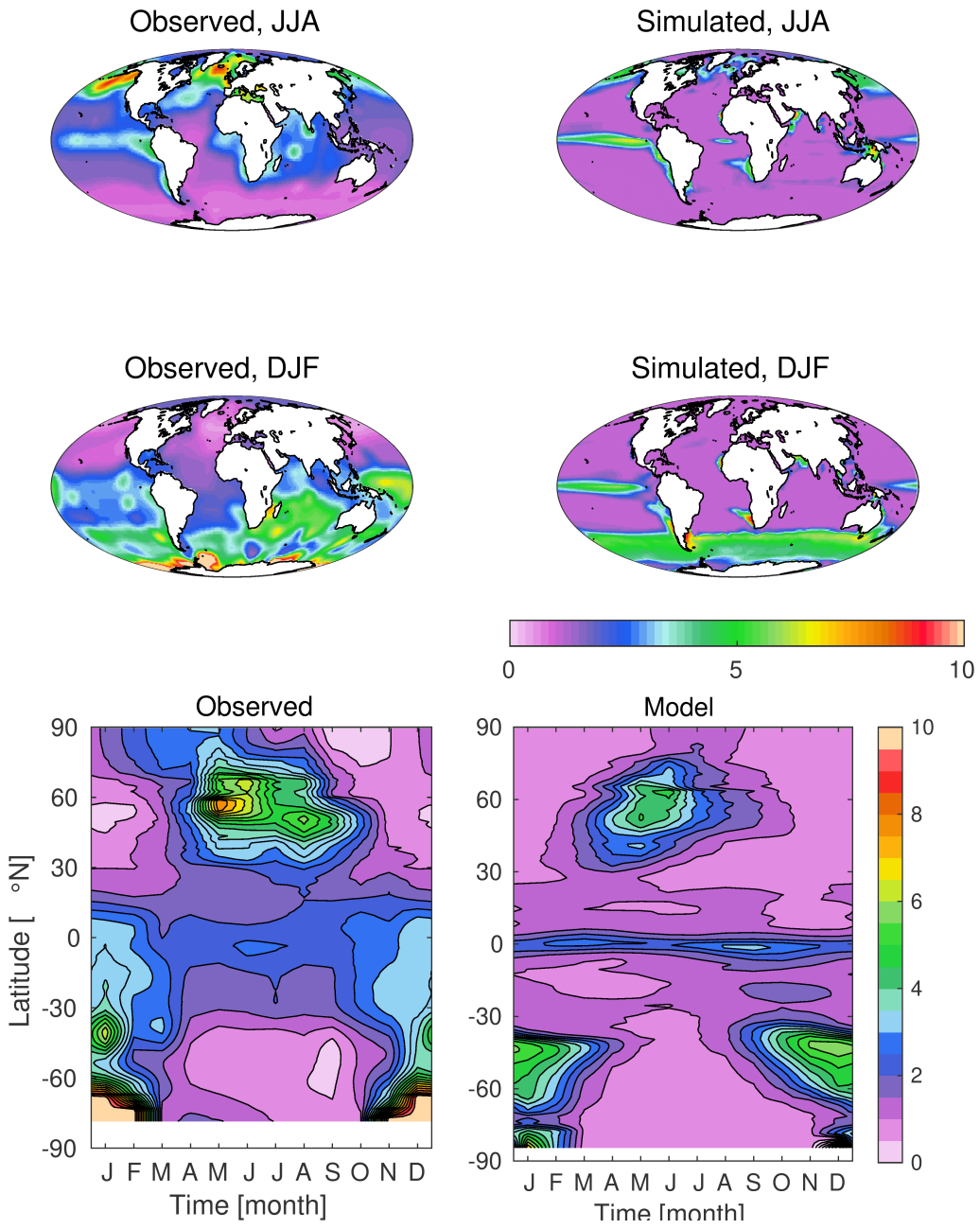

Figure S13. Observed (left; Lana et al. (2011)) and simulated (right) surface dimethylsulfide concentration, shown geographically for northern (top; JJA)and southern summer (middle; DJF), and as zonal Hovmöller diagrams (bottom). DMS concentration in μmol S m^{-3}.

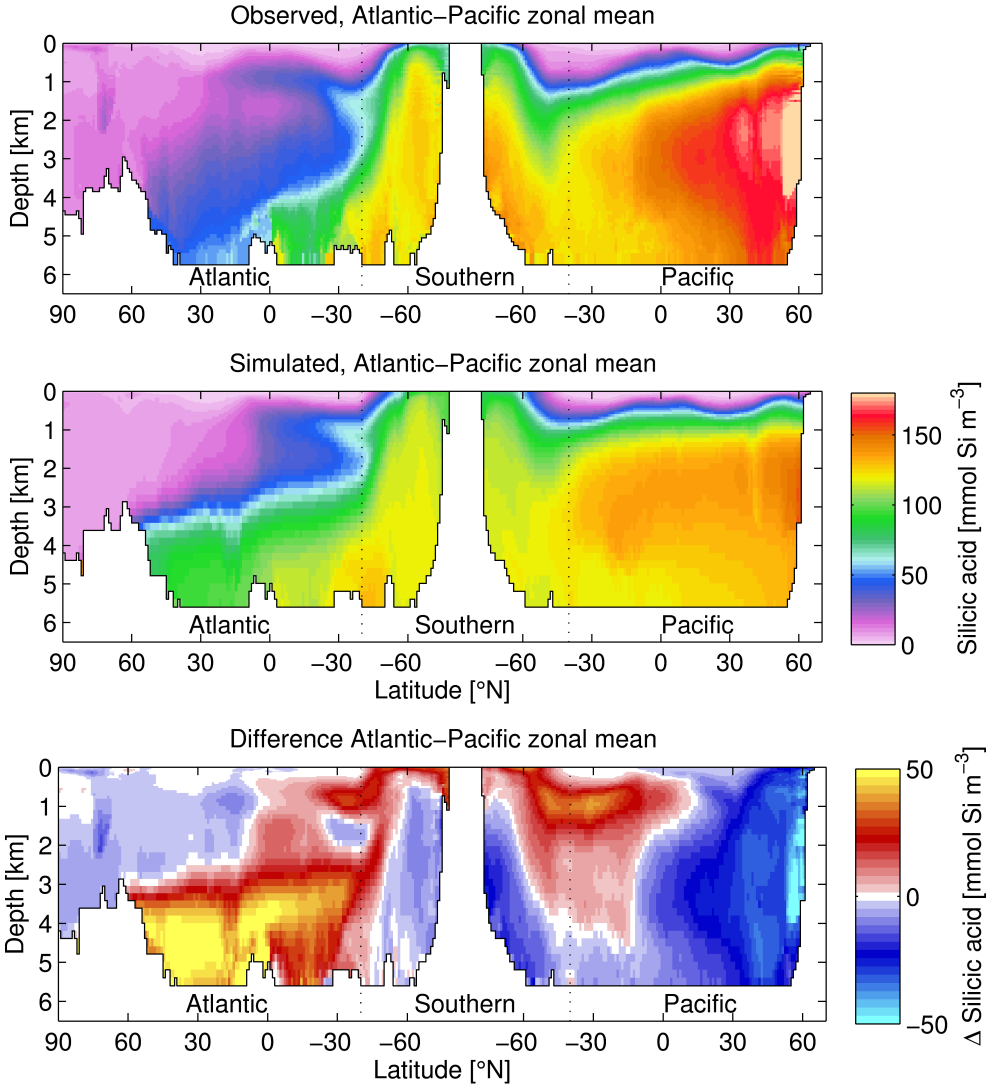

Figure S14. A "thermohaline circulation" section of observed (top) and modelled (bottom) zonal average silicic acid. Figure 6 explains the format of this section. Concentrations in mmol Si m^{-3}.

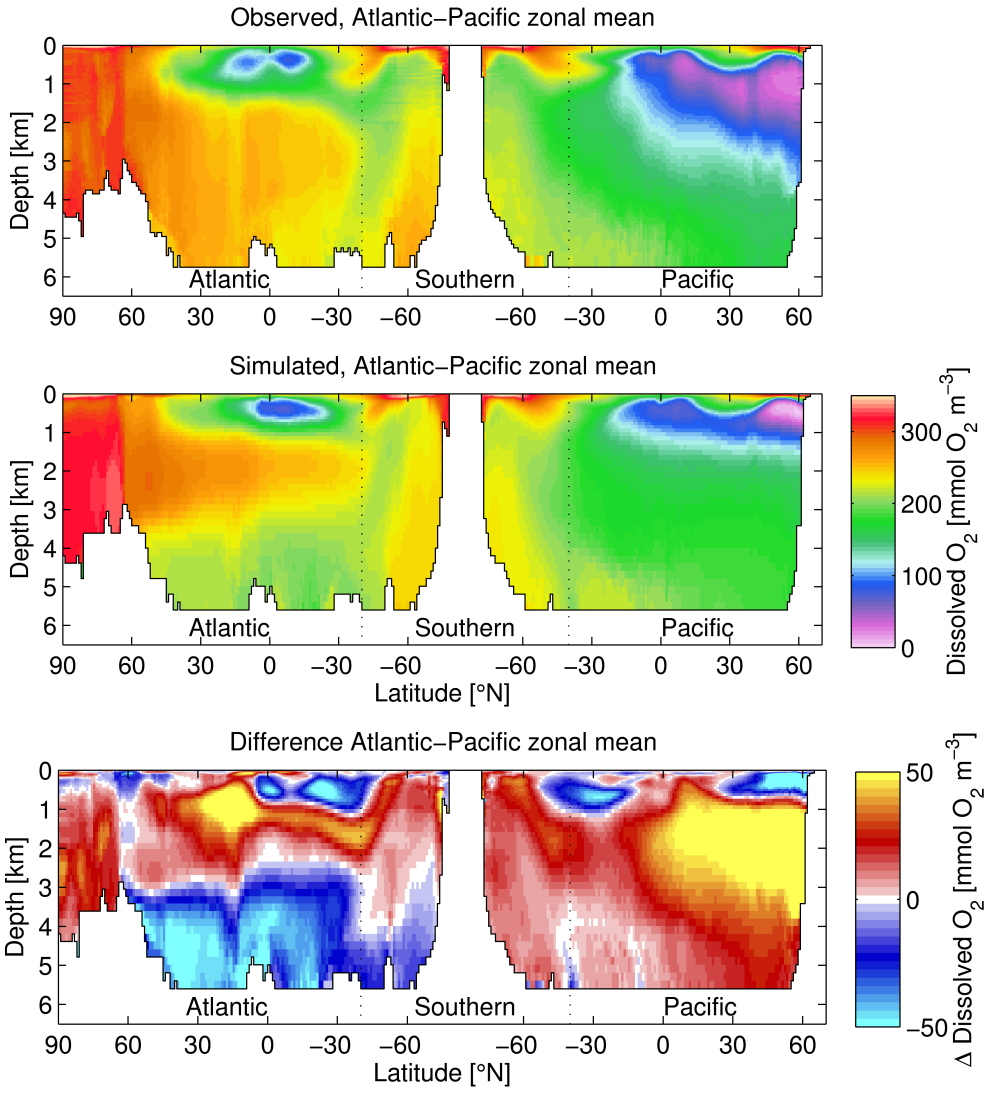

Figure S15. A "thermohaline circulation" section of observed (top) and modelled (bottom) zonal average dissolved oxygen. Figure 6 explains the format of this section. Concentrations in mmol O_2 m^{-3}.

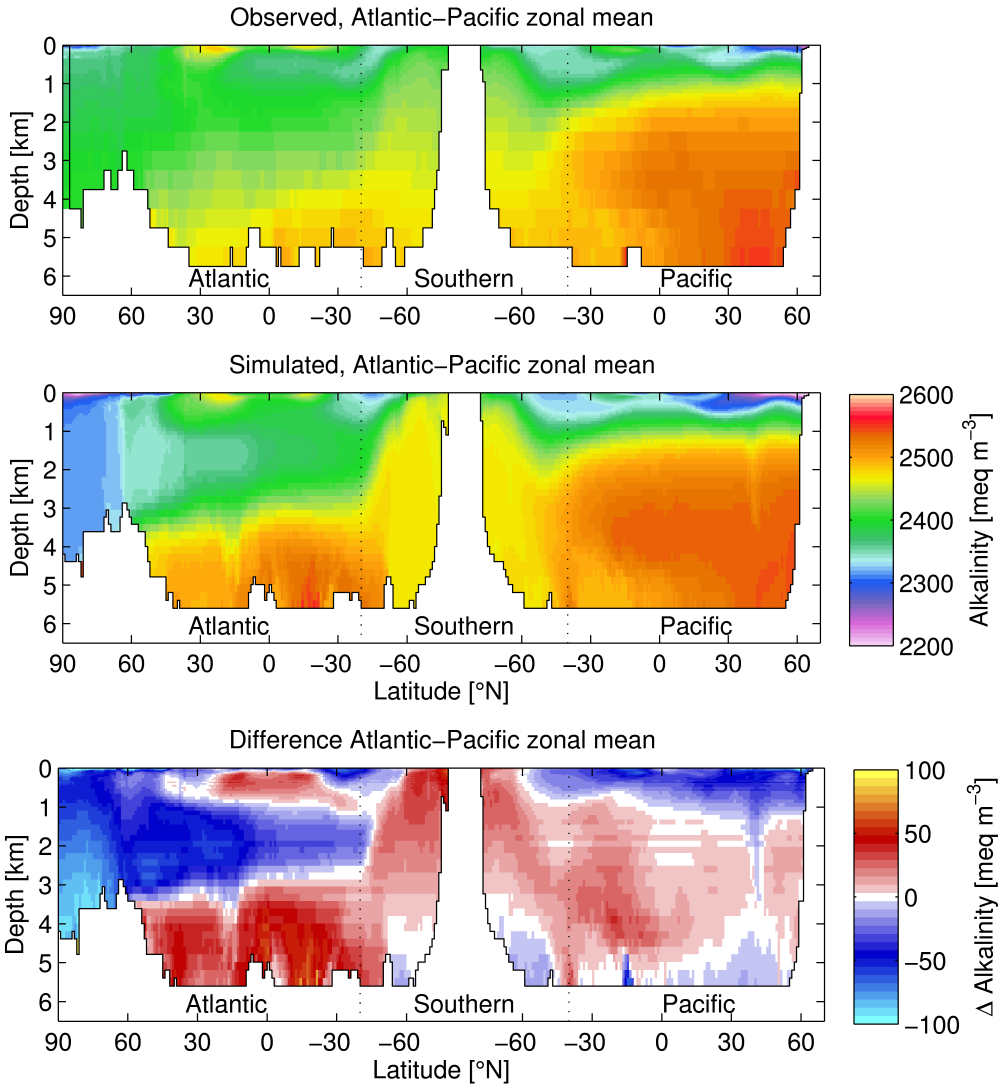

Figure S16. A "thermohaline circulation" section of observed (top) and modelled (bottom) zonal average alkalinity. Figure 6 explains the format of this section. Concentrations in meq m^{-3}.

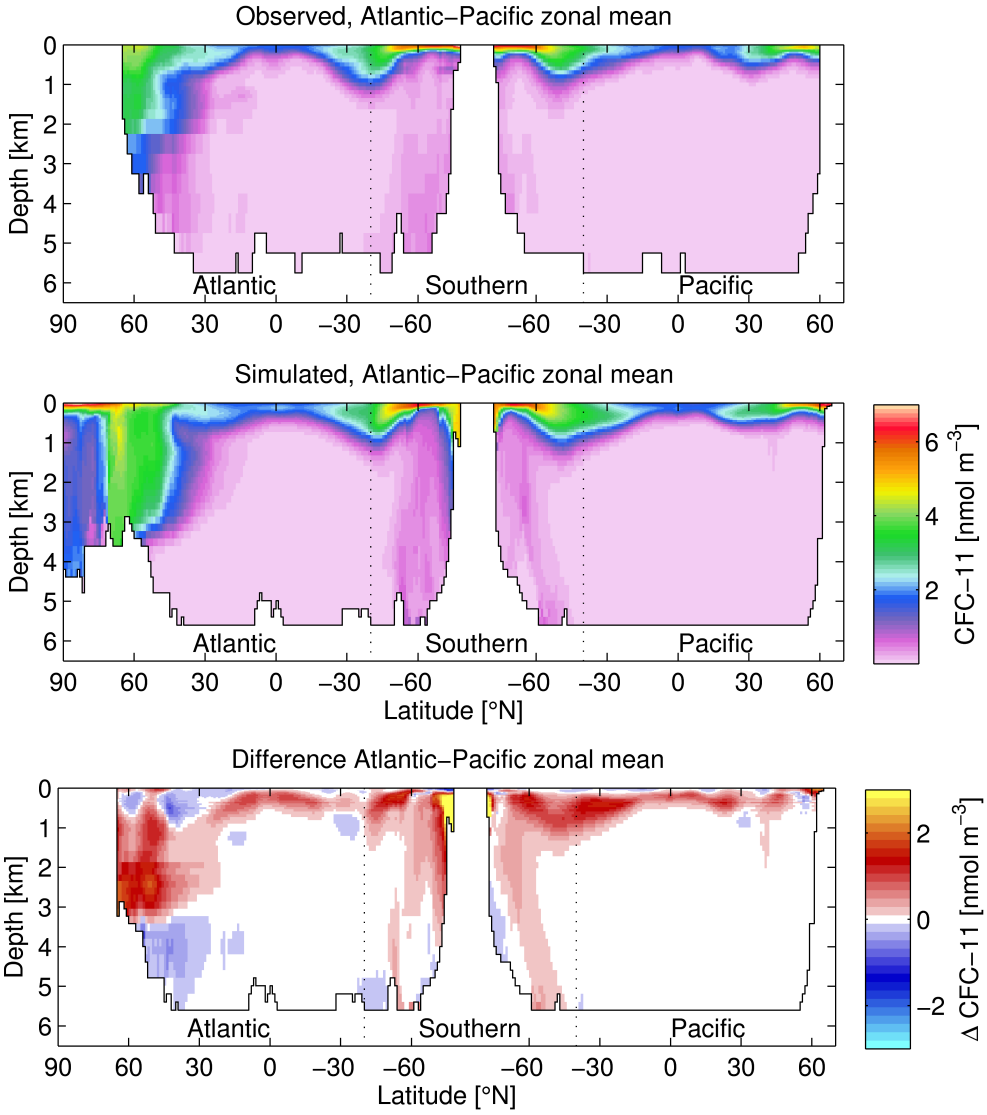

Figure S17. A "thermohaline circulation" section of observed (top) and modelled (bottom) zonal average CFC-11. Figure 6 explains the format of this section. Concentrations in nmol m^{-3}.

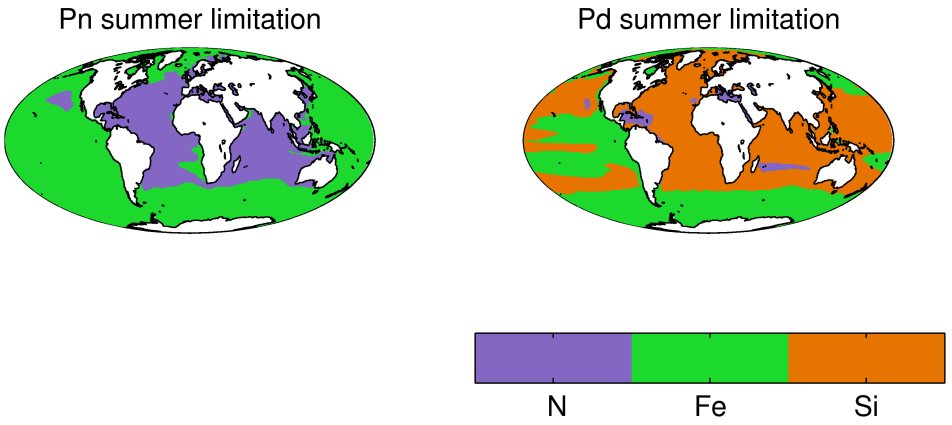

Figure S18. Simulated patterns of most-limiting nutrient for non-diatom (left; N and Fe) and diatom (right; N, Si and Fe) phytoplankton. Limitation is summertime mean, weighted by biomass and integrated for the full water column.

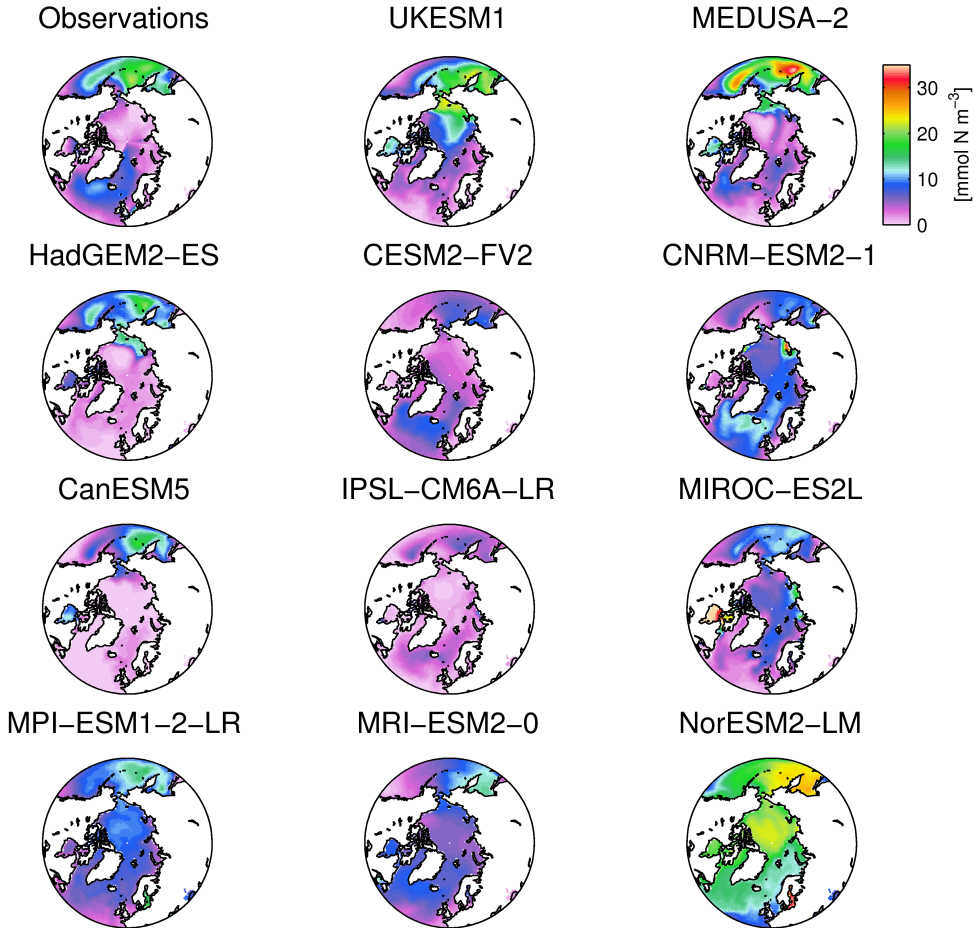

Figure S19. Intercomparison of annual mean surface dissolved inorganic nitrogen concentration in the Arctic between observed (top row, left), UKESM1 simulated (top row, centre) and a range of comparable CMIP6 models (rows 2–4). DIN concentration in mmol N m^{-3}. Previously published results from MEDUSA–2 (Yool et al., 2013) are shown for comparison (top row, right).

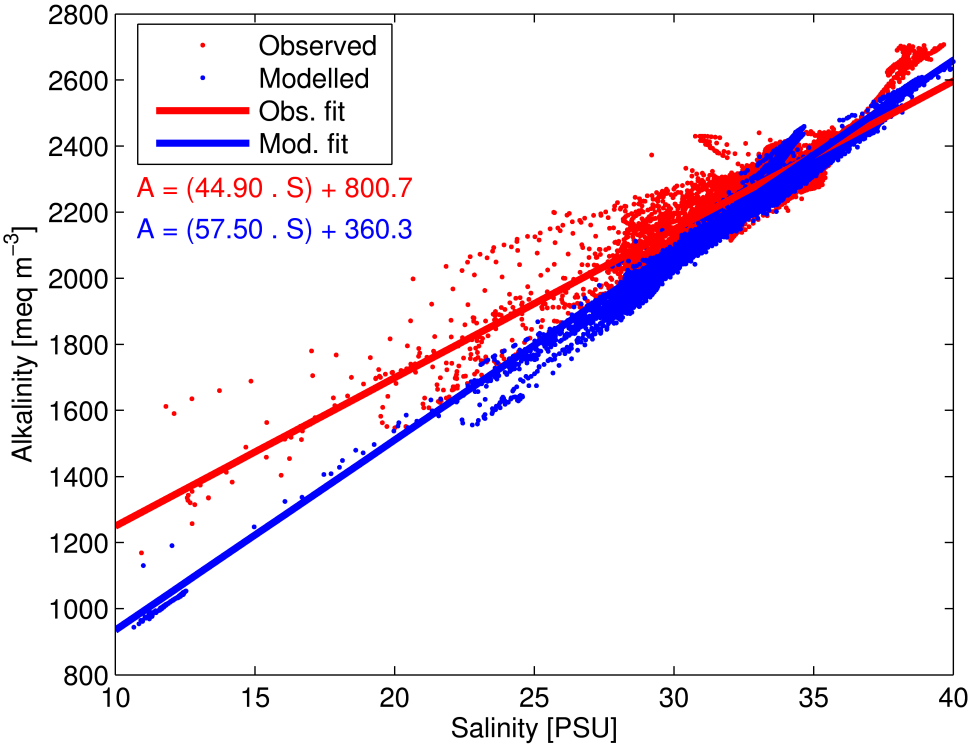

Figure S20. Surface alkalinity plotted against surface salinity for observations (red dots) and model (blue dots). Lines are corresponding linear regressions, with equations shown below legend. Salinity in PSU, alkalinity in meq m^{-3}.

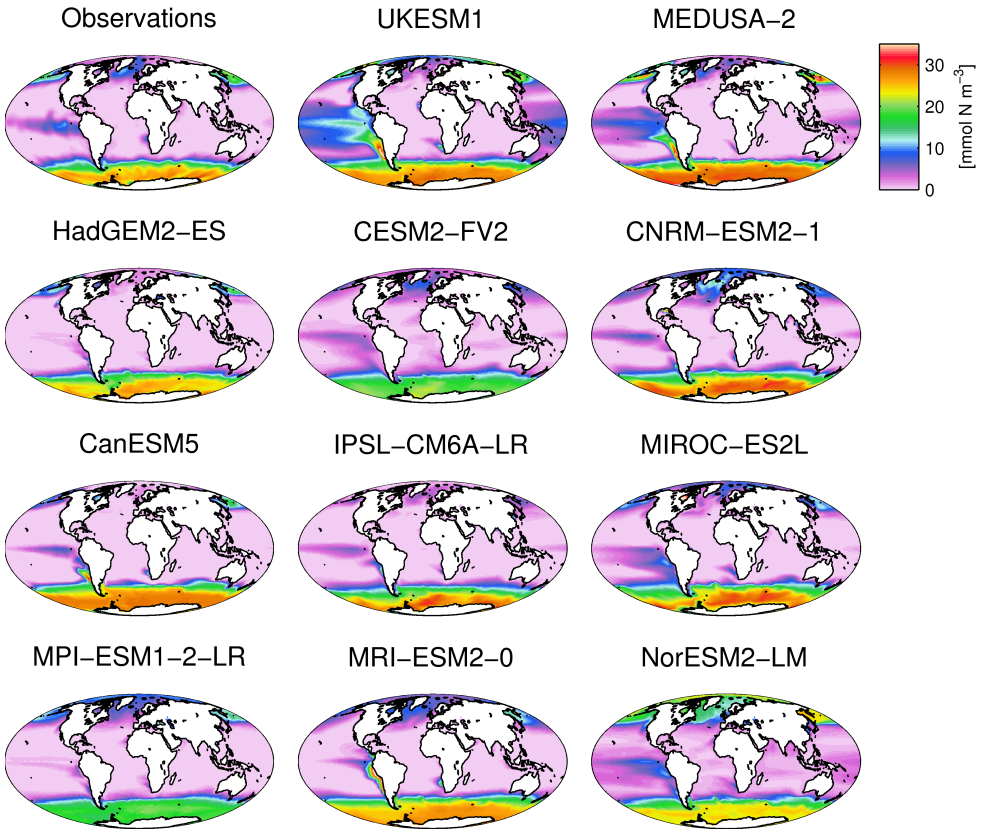

Figure S21. Intercomparison of annual mean surface dissolved inorganic nitrogen concentration between observed (top row, left), UKESM1 simulated (top row, centre) and a range of comparable CMIP6 models (rows 2–4). DIN concentration in mmol N m^{-3}. Results from CMIP5's precursor to UKESM1, HadGEM2-ES (Jones et al., 2011; row 2, left) and MEDUSA–2 (Yool et al., 2013; top row, right) are shown for comparison.

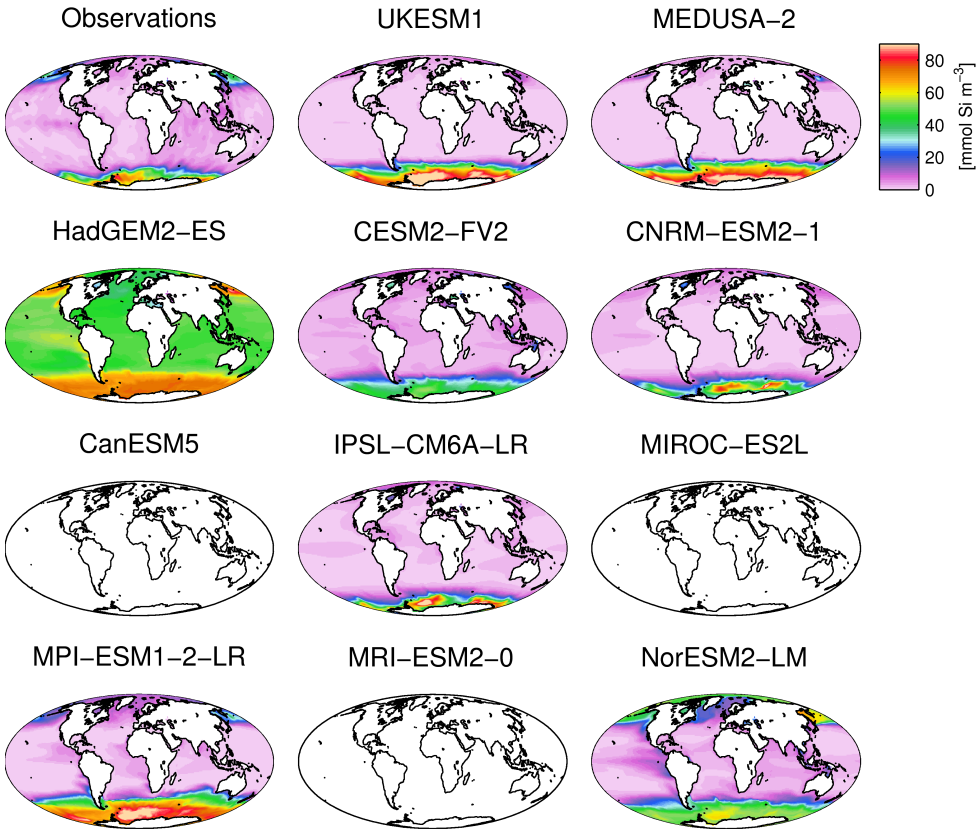

Figure S22. Intercomparison of annual mean surface silicic acid concentration between observed (top row, left), UKESM1 simulated (top row, centre) and a range of comparable CMIP6 models (rows 2–4). Results from CMIP5's precursor to UKESM1, HadGEM2-ES (Jones et al., 2011; row 2, left) and MEDUSA–2 (Yool et al., 2013; top row, right) are shown for comparison. Silicic acid concentration in mmol Si m^{-3}.

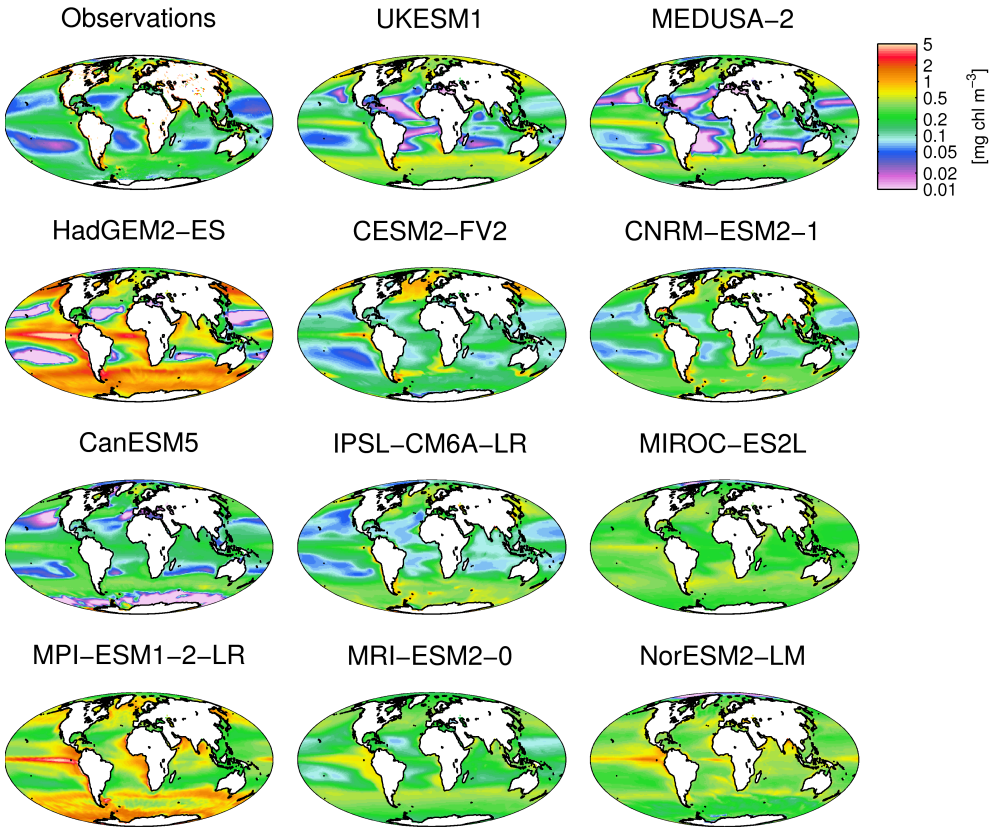

Figure S23. Intercomparison of annual mean surface chlorophyll concentration between observed (top row, left), UKESM1 simulated (top row, centre) and a range of comparable CMIP6 models (rows 2–4). Results from CMIP5's precursor to UKESM1, HadGEM2-ES (Jones et al., 2011; row 2, left) and MEDUSA–2 (Yool et al., 2013; top row, right) are shown for comparison. Chlorophyll concentration in mg chl m^{-3}.

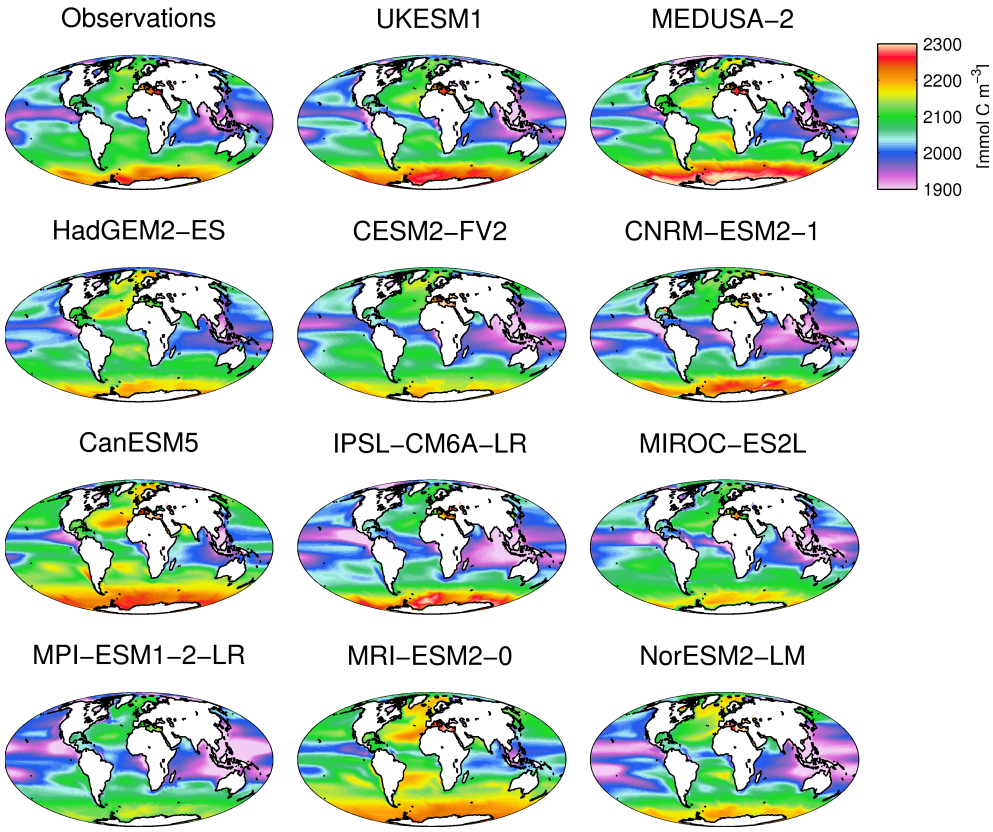

Figure S24. Intercomparison of annual mean surface dissolved inorganic carbon concentration between observed (top row, left), UKESM1 simulated (top row, centre) and a range of comparable CMIP6 models (rows 2–4). Results from CMIP5's precursor to UKESM1, HadGEM2-ES (Jones et al., 2011; row 2, left) and MEDUSA–2 (Yool et al., 2013; top row, right) are shown for comparison. DIC concentration in mmol C m^{-3}.

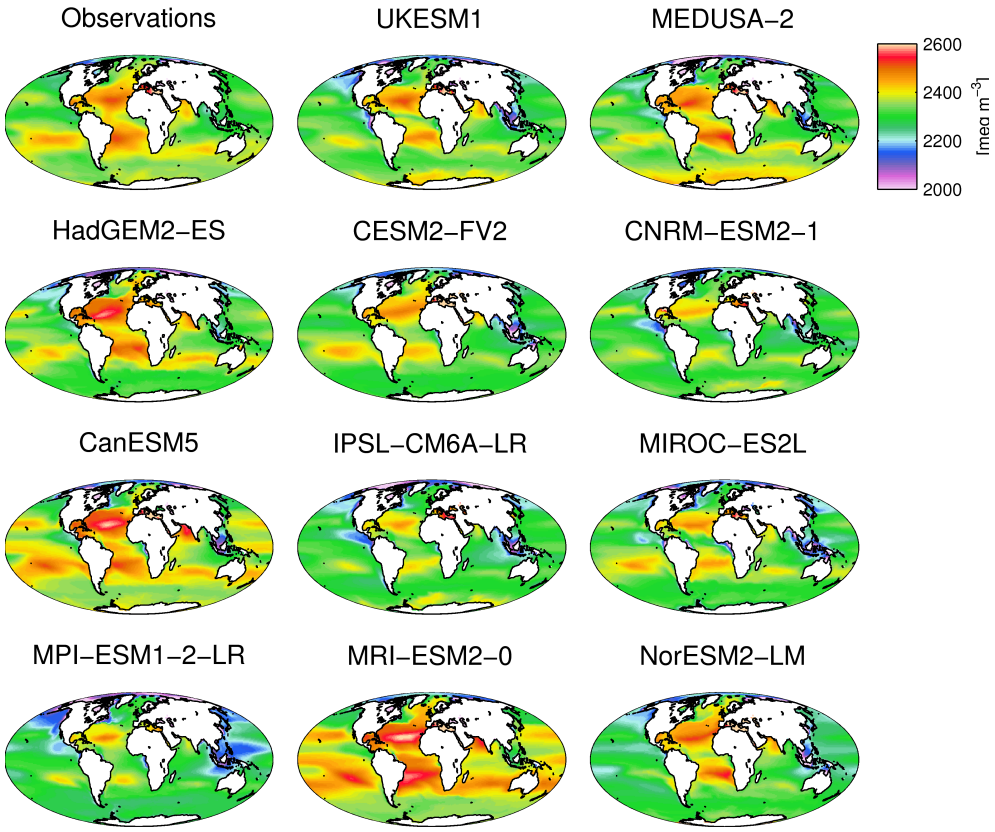

Figure S25. Intercomparison of annual mean surface alkalinity between observed (top row, left), UKESM1 simulated (top row, centre) and a range of comparable CMIP6 models (rows 2–4). Results from CMIP5's precursor to UKESM1, HadGEM2-ES (Jones et al., 2011; row 2, left) and MEDUSA–2 (Yool et al., 2013; top row, right) are shown for comparison. Alkalinity in meq m^{-3}.

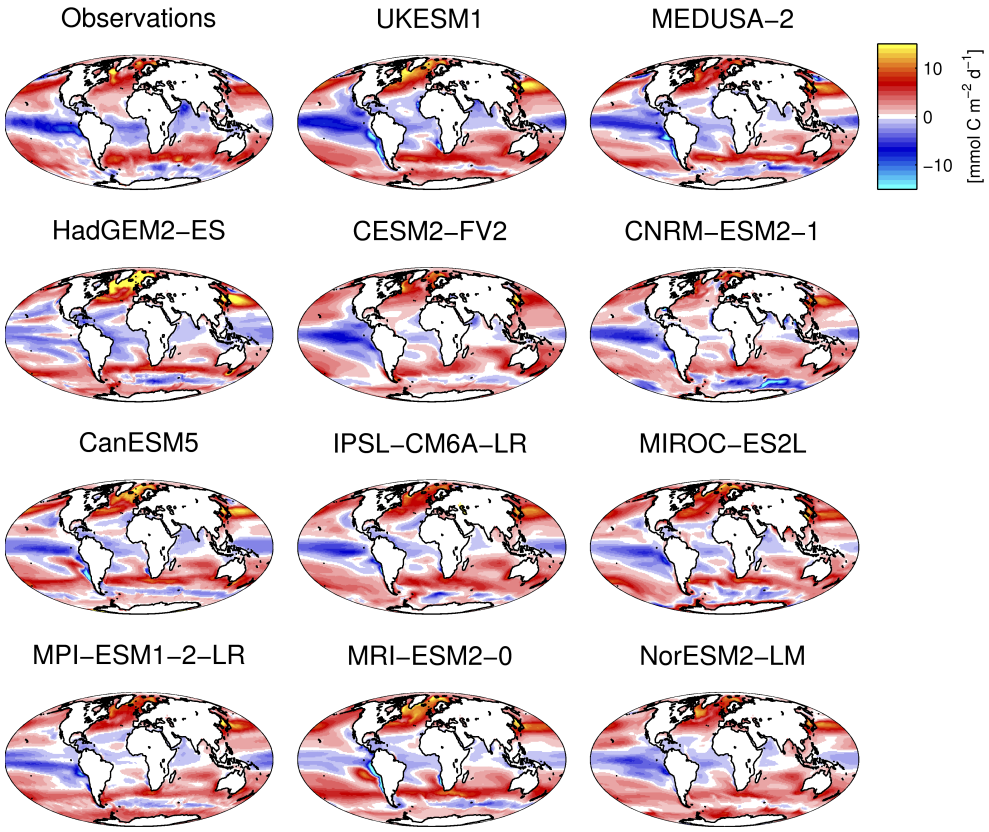

Figure S26. Intercomparison of annual mean air-sea CO_2 flux between observed (top row, left), UKESM1 simulated (top row, centre) and a range of comparable CMIP6 models (rows 2–4). Results from CMIP5's precursor to UKESM1, HadGEM2-ES (Jones et al., 2011; row 2, left) and MEDUSA–2 (Yool et al., 2013; top row, right) are shown for comparison. Red / blue colours respectively indicate flux into / out of the ocean. CO_2 flux in mmol C m^{-2} d^{-1}.

#	Run ID	Branch point	Ensemble ID
0	*u-aw310*	–	–
1	u-az513	170 y	r5i1p1f2
2	u-az515	200 y	r6i1p1f2
3	u-az524	145 y	r7i1p1f2
4	u-bb075	110 y	r4i1p1f2
5	u-bb277	710 y	r8i1p1f2
6	u-bc179	400 y	r1i1p1f2
7	u-bc292	315 y	r2i1p1f2
8	u-bc370	270 y	r3i1p1f2
9	u-bc470	435 y	r9i1p1f2

Table S1. Historical ensemble members used in this study. Run IDs are the formal job identification tags of the ensemble members on local systems, and can be used to access full model outputs on the MASS archive system. The branch points indicate the time points of the piControl simulation from which model states were taken to initialise the ensemble members. The ensemble IDs are the experimental variant identifiers used in the ESGF. Note that the table is ordered by run ID and not branch point time.

Model name	Institution code	Variant	Further information
HadGEM2-ES	MOHC	r1i1p1	(CMIP5 precursor to UKESM1)
CESM2-FV2	NCAR	r1i1p1r1	https://furtherinfo.es-doc.org/CMIP6.NCAR.CESM2-FV2.historical.none.r1i1p1f1
CNRM-ESM2-1	CNRM-CERFACS	r1i1p1f2	https://furtherinfo.es-doc.org/CMIP6.CNRM-CERFACS.CNRM-ESM2-1.historical.none.r1i1p1f2
CanESM5	CCCma	r1i1p1f1	https://furtherinfo.es-doc.org/CMIP6.CCCma.CanESM5.historical.none.r1i1p1f1
IPSL-CM6A-LR	IPSL	r32i1p1f1	https://furtherinfo.es-doc.org/CMIP6.IPSL.IPSL-CM6A-LR.historical.none.r32i1p1f1
MIROC-ES2L	MIROC	r1i1p1f2	https://furtherinfo.es-doc.org/CMIP6.MIROC.MIROC-ES2L.historical.none.r1i1p1f2
MPI-ESM1-2-LR	MPI-M	r1i1p1f1	https://furtherinfo.es-doc.org/CMIP6.MPI-M.MPI-ESM1-2-LR.historical.none.r1i1p1f1
MRI-ESM2-0	MRI	r1i2p1f1	https://furtherinfo.es-doc.org/CMIP6.MRI.MRI-ESM2-0.historical.none.r1i2p1f1
NorESM2-LM	NCC	r1i1p1f1	https://furtherinfo.es-doc.org/CMIP6.NCC.NorESM2-LM.historical.none.r1i1p1f1

Table S2. CMIP6 models used in Figures 23 and 24, and Supplementary Figures S21 to S26. Model institution codes, variants and further information links are given for each model. References for models are given in the main body of the manuscript.